J Therm Anal Calorim (2010) 100:33–42
DOI 10.1007/s10973-009-0188-z

Finite-difference model for the reaction sintering of oxide ceramics by direct oxidation of intermetallic powder compacts

H. Geßwein · N. Schlechtriemen · J. R. Binder · J. Haußelt

Received: 10 March 2009 / Accepted: 22 April 2009 / Published online: 19 June 2009

Abstract A kinetic model for the reaction sintering of oxide ceramics in the system Al_2O_3–SiO_2–ZrO_2 using mixtures of intermetallic compounds is presented. A 2D finite-difference model is developed to describe the exothermic gas-solid reactions taking place during the firing of $ZrAl_3$/$ZrSi_2$ powder compacts. The model accounts for the oxidation kinetics of the powder particles, as well as the consumption and diffusion of gaseous oxygen through the porous matrix. Additionally, possible changes in the pore structure of the green body due to the oxidation reactions and sintering effects are incorporated in the model. The resulting differential equations are coupled with a two-dimensional Fourier heat balance equation leading to a system of nonlinear partial differential equations, which is solved by the numerical method of lines. The influence of different processing parameters like sample composition and heating cycle on the reaction sintering process is investigated and the model-predicted reaction behaviour is compared to experimental results.

Keywords Kinetics · Model fitting · Oxidation · Thermogravimetric analysis · Simulation

Introduction

The fabrication of advanced ceramic materials by reaction sintering techniques is an established ceramic processing method which offers a number of advantages such as near-net shape capability compared with conventional processing routes [1]. Important engineering ceramics such as SiC and Si_3N_4 in the case of non-oxide ceramics as well as structural oxide ceramics like Al_2O_3 or mullite can be reaction-formed. In general, reaction sintering processes can be divided into gas–solid, solid–solid and liquid–gas reactions. Heterogeneous gas–solid reactions involving the reaction of a metal and a gaseous oxidant are usually extremely exothermic and a large amount of heat can be liberated during the oxidation reaction. As a result, local overheating of the compacted green bodies, which can amount to several hundred degrees Celsius, may be observed. This uncontrolled reaction behaviour leads to typical processing problems like sample cracking and bloating and careful temperature control must be accomplished to assure the production of defect-free high quality ceramics. The thermal response of the reactive sample is governed by the interaction of the heat release due to the exothermic oxidation reactions and the rate of heat loss from the surface of the sample to the surroundings. Therefore, the detailed knowledge of the oxidation kinetics of the reactive solids is an essential prerequisite for processing understanding, modeling and control.

The use of intermetallic compounds in the systems Zr–Al and Zr–Si offers the advantage of a much higher volume increase during oxidation compared to pure metals like aluminum or zirconium and thus, the sintering shrinkage can be completely compensated [2, 3]. This enables the fabrication of net shape reaction bonded ceramic parts by mechanical structuring in the green state [4]. Using a combination of $ZrAl_3$ and $ZrSi_2$ as reactive precursor materials leads to the formation of ceramics belonging to the ternary phase diagram Al_2O_3–SiO_2–ZrO_2. By adjusting the initial composition of the green body, i.e. the Zr/Al/Si ratio, the phase composition of the final sintered ceramic can be varied over a wide range. The overall oxidation

H. Geßwein (✉) · N. Schlechtriemen · J. R. Binder · J. Haußelt
Institute for Materials Research III, Forschungszentrum Karlsruhe GmbH, P.O. 3640, 76021 Karlsruhe, Germany
e-mail: holger.gesswein@imf.fzk.de

reactions taking place during reaction sintering can be summarised as follows:

$$ZrAl_{3(s)} + 13/4O_{2(g)} \rightarrow ZrO_{2(s)} + 3/2Al_2O_{3(s)} \quad (1)$$

$$ZrSi_{2(s)} + 3O_{2(g)} \rightarrow ZrO_{2(s)} + 2SiO_{2(s)} \quad (2)$$

Because of the high mass changes involved in these oxidation reactions, thermogravimetry is suited for the kinetic study and the determination of the "kinetic triplet" (i.e. Arrhenius parameters E_a and A and the reaction model $f(\alpha)$). As was shown recently by Burnham [5] isoconversional and model-fitting approaches can yield comparable results if a combination of isothermal and constant heating rate data is used for the derivation of the kinetic parameters. The advantage of the model-fitting kinetic approach is that the determined kinetic models which describe the oxidation reactions of the powder particles can be readily incorporated in more detailed reaction-diffusion models where the mass balances of the reacting solids and gaseous oxidants are coupled with a transient energy balance equation. A similar modelling approach was already used for the advanced kinetic description of the decomposition of energetic materials [6].

Aims of this work are to extend the already proposed model [7] by including suitable oxidation kinetics of the two different intermetallic compounds and possible changes in the pore-structure due to sintering effects. The model can then be used to study the oxidation behaviour of compacted powder samples of different sizes and compositions under any programmed temperature profiles and for thermal process optimization, i.e. the reduction of the processing time of the cost intensive thermal treatment. This is an important issue for potential industrial applications of these reaction sintered oxide ceramics.

Model formulation

The model equations formulated here describe the oxidation process of compacted powder mixtures of the intermetallic compounds $ZrAl_3$ and $ZrSi_2$. The schematic representation of the sample with the selected spatial reference system is shown in Fig. 1. Inside the sample, reactions between the gaseous oxidizer and the particles of the solid reactants occur according to Eqs. 1 and 2. These reactions occur at the particle level. Hence, one must use suitable models for the oxidation kinetics of the powder particles. In addition the effect of oxygen supply and consumption has to be considered. Oxygen has to diffuse into the porous matrix of the solids to be available for the reaction to proceed. The oxidation kinetics of the intermetallics, microstructural changes of the samples as well as additional assumptions which have been made, are described in the following paragraphs.

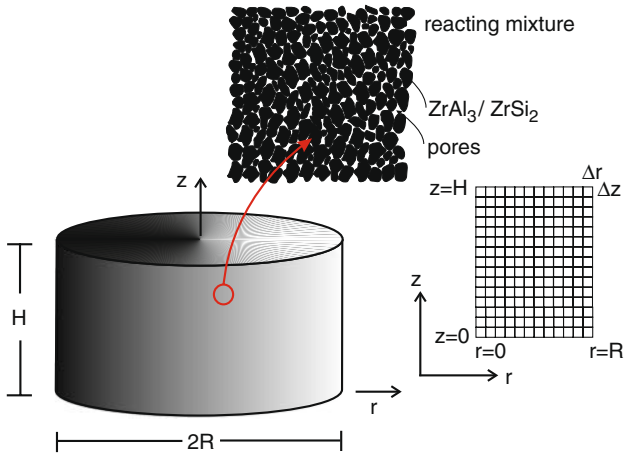

Fig. 1 Schematic representation of the reacting sample used for the modelling

Oxidation kinetics

The rate of solid-state or heterogeneous processes can be generally described by:

$$\frac{d\alpha}{dt} = k(T)f(\alpha) = A\exp\left(-\frac{E_a}{RT}\right)f(\alpha) \quad (3)$$

where $f(\alpha)$ is a function of the degree of conversion, t is the time, T is the temperature, $k(T)$ is the rate constant, A is the pre-exponential factor, E_a is the apparent activation energy and R is the gas constant. If gaseous reactants or products are involved in the reaction, a function of their concentrations $f_2(C_g)$ is included in Eq. 3. The functions $f(\alpha)$ and $f_2(C_g)$ originate from physico-geometric considerations and/or the law of mass action. For examples of the most common $f(\alpha)$ functions used in heterogeneous kinetics see Brown et al. [8]. The oxidation kinetics of $ZrAl_3$ and $ZrSi_2$ powders were studied in detail in previous papers [9, 10]. In these studies care was taken to determine the intrinsic oxidation kinetics unaffected by diffusional and mass transfer effects. Table 1 summarises the experimentally determined kinetic models and parameters for the two oxidation reactions. The $ZrAl_3$ oxidation can be well described with a generalized n-dimensional Avrami type rate equation (An) indicating a diffusion-limited process where oxide nuclei are initially present and the growth process is one-dimensional with diffusion-control [11]. The oxidation process of $ZrSi_2$ powders is a complex gas-solid reaction with multi-step character. During $ZrSi_2$ oxidation two concurrent oxidation mechanisms with the formation of intermediate reaction products occur. In one reaction pathway $ZrSi_2$ is selectively oxidized to ZrO_2 and Si. The other pathway is described by the non-selective oxidation of $ZrSi_2$ to ZrO_2 and SiO_x. At higher temperatures the selectively formed Si is further oxidized in a third step.

Table 1 Kinetic models, schematic reaction schemes and kinetic parameters for the oxidation of $ZrAl_3$ and $ZrSi_2$ powders [9, 10]. For the definition of the kinetic parameters see [18]

Material	Kinetic model, reaction types and kinetic parameters
$ZrAl_3$	Single step oxidation model described by generalized n-dimensional Avrami type rate equation (An) according to a diffusion limited growth reaction: $A \xrightarrow{1} B$
	$f(\alpha)$: An, $\lg(A/s^{-1}) = 9.45$, $E_a = 244$ kJ/mol, $n = 0.34$
$ZrSi_2$	Complex gas–solid oxidation reaction. Best fit model consists of three-step branching reaction model based on 3D diffusion (D3F) and fractal order reaction (Fn):
	$A \xrightarrow{1} B$
	$A \xrightarrow{2} C \xrightarrow{3} B$
	Step 1: D3F, $\lg(A_1/s^{-1}) = 0.77$, $E_{a1} = 125$ kJ/mol
	Step 2: D3F, $\lg(A_2/s^{-1}) = 8.36$, $E_{a2} = 257$ kJ/mol
	Step 3: D3F, $\lg(A_3/s^{-1}) = 2.93$, $E_{a3} = 170$ kJ/mol, $n = 2.3$

According to this formal kinetic model following notation for the $ZrSi_2$ oxidation kinetics is used throughout this paper:

- $ZrSi_2$-A: oxidation educt ($ZrSi_2$)
- $ZrSi_2$-B: final oxidation product (ZrO_2 and SiO_2)
- $ZrSi_2$-C: intermediate oxidation product (Si and SiO_x)

Simultaneous energy and mass balance

Heat production and dissipation play an important role in the reaction of a porous reactive solid and a gaseous oxidant. In this study a two-dimensional cylindrical model for heat-transfer, modified to allow for heat generation by chemical reactions with specified kinetics is used to simulate the programmed heating of compacted $ZrAl_3/ZrSi_2$ powder mixtures in a conventional box furnace. The generalized transient two-dimensional energy balance coupled with kinetic rate functions and reaction heat terms can be written as:

$$(1-\varepsilon_m)\rho_m c_{p,m}\frac{\partial T}{\partial t} = k_m\left(\frac{\partial^2 T}{\partial z^2}+\frac{1}{r}\frac{\partial T}{\partial r}+\frac{\partial^2 T}{\partial r^2}\right) + (1-\varepsilon_m)\sum_i w_i\rho_i Q_i\frac{\partial C_i}{\partial t} \quad (4)$$

where t is the time variable, T is the temperature, r and z are the spatial coordinates, Q_i are the chemical heats generated by the oxidation reactions, w_i are the weight fractions of the intermetallic compounds in the green body and ρ_i are the densities of the different species i (i.e. $ZrAl_3$ and $ZrSi_2$). It is assumed that the heat transfer rate between the solid and the gas is sufficiently large to adopt the same temperature field for both. Material parameters are the thermal conductivity k_m, specific heat $c_{p,m}$, theoretical density ρ_m and the porosity ε_m of the compacted powder mixture. The chemical rate equations for the different oxidation reactions of the solid reactants according to the experimentally determined kinetic models as well as the mass balance for the gaseous oxidant can be written as:

$$\frac{\partial C_{ZrAl_3}}{\partial t} = -k(T)f(C_{ZrAl_3})f_2(C_g) \quad (5)$$

$$\frac{\partial C_{ZrSi_2-A}}{\partial t} = -k_1(T)f(C_{ZrSi_2-A})f_2(C_g) - k_2(T)f(C_{ZrSi_2-A})f_2(C_g) \quad (6)$$

$$\frac{\partial C_{ZrSi_2-B}}{\partial t} = k_1(T)f(C_{ZrSi_2-A})f_2(C_g) + k_3(T)f(C_{ZrSi_2-C})f_2(C_g) \quad (7)$$

$$\frac{\partial C_{ZrSi_2-C}}{\partial t} = k_2(T)f(C_{ZrSi_2-A})f_2(C_g) - k_3(T)f(C_{ZrSi_2-C})f_2(C_g) \quad (8)$$

$$\frac{\partial C_g}{\partial t} = D_e\left(\frac{\partial^2 C_g}{\partial z^2}+\frac{1}{r}\frac{\partial C_g}{\partial r}+\frac{\partial^2 C_g}{\partial r^2}\right) - w_{ZrAl_3}\gamma_{ZrAl_3}k(T)f(C_{ZrAl_3})f_2(C_g) - w_{ZrSi_2}\gamma_{ZrSi_2}\left[k_1(T)f(C_{ZrSi_2-A})f_2(C_g) + k_2(T)f(C_{ZrSi_2-A})f_2(C_g) + k_3(T)f(C_{ZrSi_2-C})f_2(C_g)\right] \quad (9)$$

where D_e is an effective diffusion coefficient and the stoichiometric coefficients $\gamma_i = (1-\varepsilon_{m,0})\rho_i/\rho_g$ describe the ratio of the densities of the solids i (i.e. $ZrAl_3$ and $ZrSi_2$) and oxygen gas. C_{ZrAl3} and C_g are the relative concentrations of $ZrAl_3$ and oxygen, respectively. $C_{ZrSi2\text{-}A}$, $C_{ZrSi2\text{-}C}$ and $C_{ZrSi2\text{-}B}$ are, according to the formal oxidation reaction scheme presented in Table 1, the relative concentrations of the educt, intermediate reaction product and final product of the $ZrSi_2$ oxidation reaction. The density of oxygen is given by the ideal gas law as $p_{O2}M_{O2}/RT$, where M_{O2} and p_{O2} are the molecular mass and partial pressure of oxygen, respectively. For atmospheric pressure ρ_g is 0.27 kg/m^3 (assuming p_{O2} is 0.21×10^5 Pa). In addition, the dependencies of the thermophysical properties such as heat capacity and thermal conductivity on temperature and compositions are taken as:

$$c_{p,m}(T) = \sum\nolimits_i m_i c_{p,i}(T) \quad (10)$$

$$k_m(T) = \left(\frac{\rho_m}{\rho_{th}}\right)\sum\nolimits_i v_i k_i(T) \quad (11)$$

where ρ_m is the sample density, m_i, v_i are the mass and volume fractions of the educts ($ZrAl_3$, $ZrSi_2$) and oxidation products (Al_2O_3, SiO_2, ZrO_2), and ρ_{th} is the theoretical density of the sample. The theoretical density of the reacting sample at any instant is calculated by using the mass fractions of the educts and products during the oxidation

process according to Eqs. 1 and 2 and the corresponding kinetic rate laws. Values for the heat capacities of the educts and products as a function of the temperature were taken from the literature (http://webbook.nist.gov/chemistry) otherwise the thermophysical parameters were estimated and taken as constants.

As a first approximation the overall reaction rates are assumed to be of first order in the oxygen concentration ($f_2(C_g) = C_g$). Thus, the oxidation reactions take place whenever the concentration functions of the solids and gaseous oxidant are different from zero. Within this assumption the consumption of oxygen in the void space, is taken into account, but it has to be mentioned that this expression is empirical and does not attempt to describe the exact influence of the oxygen partial pressure on the reaction mechanism. Another simplification is that phase formation reactions, i.e. the formation of zircon and/or mullite, which may take place after the oxidation reactions are not accounted for.

The boundary conditions, as shown in Fig. 1, for the temperature and relative oxygen concentration are:

$$k\frac{\partial T}{\partial r}\bigg|_{r=0} = 0, D_e\frac{\partial C_g}{\partial r}\bigg|_{r=0} = 0 \tag{12}$$

$$\begin{aligned} k\frac{\partial T}{\partial z}\bigg|_{z=0} &= -[h(T_a - T) + \sigma\varepsilon(T_a^4 - T^4)], \\ D_e\frac{\partial C_g}{\partial z}\bigg|_{z=0} &= -k_g[(C_{g,a} - C_g)] \end{aligned} \tag{13}$$

$$\begin{aligned} k\frac{\partial T}{\partial z}\bigg|_{z=H} &= [h(T_a - T) + \sigma\varepsilon(T_a^4 - T^4)], \\ D_e\frac{\partial C_g}{\partial z}\bigg|_{z=H} &= k_g[(C_{g,a} - C_g)] \end{aligned} \tag{14}$$

$$\begin{aligned} k\frac{\partial T}{\partial r}\bigg|_{r=R} &= [h(T_a - T) + \sigma\varepsilon(T_a^4 - T^4)], \\ D_e\frac{\partial C_g}{\partial r}\bigg|_{r=R} &= -k_g[(C_{g,a} - C_g)] \end{aligned} \tag{15}$$

with the initial conditions

$$C_{\mathrm{ZrAl_3}}(r,z,0) = 1.0, \quad C_g(r,z,0) = 1.0, \quad T(r,z,0) = T_0 \tag{16}$$

$$C_{\mathrm{ZrSi_2-A}}(r,z,0) = 1.0 \tag{17}$$

$$C_{\mathrm{ZrSi_2-B}}(r,z,0) = 0.0 \tag{18}$$

$$C_{\mathrm{ZrSi_2-C}}(r,z,0) = 0.0 \tag{19}$$

h is the heat transfer coefficient, k_g is an overall mass transfer coefficient, ε the emissivity of the sample, σ is the Stefan–Boltzmann constant and T_a and T_0 are the ambient and starting temperatures, respectively. Different heating cycles and furnace temperatures can be investigated by expressing the ambient temperature $T_\mathrm{a} = T_\mathrm{a}(t)$.

Porosity changes due to chemical reactions and sintering

During the course of the oxidation process the porosity of the powder compact changes due to both chemical reaction and sintering. The variation of porosity ε_m due to volumetric changes caused by the oxidation reactions is assumed as [12]:

$$\varepsilon_m = \varepsilon_{m,0} + (1 - \varepsilon_{m,0})(1 - Z)\alpha \tag{20}$$

where $\varepsilon_{m,0}$ is the initial porosity, Z is an expansion coefficient for the oxidation reactions and α is the overall conversion. The actual porosity change due to both chemical reaction and sintering is [13]:

$$\varepsilon_m = [\varepsilon_{m,0} + (1 - \varepsilon_{m,0})(1 - Z)\alpha](1 - \phi) \tag{21}$$

where ϕ is the fraction of pores removed by sintering. The removal of pores due to sintering is modelled as a first-order process:

$$\frac{\mathrm{d}\phi}{\mathrm{d}t} = (1 - \phi)A_s \exp\left(-\frac{E_s}{RT}\right) \tag{22}$$

The Arrhenius parameters for sintering E_s and A_s have to be estimated by independent sintering experiments on the solids and depend on the composition of the investigated samples. According to a correlation given by Ramachandran and Smith [14] the change in the effective diffusion coefficient of the compact due to combined effects of chemical reaction and sintering is:

$$D_e = \frac{D}{g(\phi)}\varepsilon_m^2 = [\varepsilon_{m,0} + (1 - \varepsilon_{m,0})(1 - Z)\alpha]^2(1 - \phi) \tag{23}$$

where the diffusion coefficient D accounts for Knudsen diffusion. The fractional increase in tortuosity of pores, $g(\phi)$, is defined as follows [15]:

$$g(\phi) = \frac{\tau_f(\phi)}{\tau_f(0)} \tag{24}$$

where $\tau_f(\phi)$ is the tortuosity factor now defined when a fraction ϕ of the porosity is removed [13]. The correlation for $g(\phi)$ as a function of ϕ is given by Ramachandran and Smith [14] was encoded into the simulation program in polynomial form.

Numerical solution

The coupled system of partial differential equations was solved with the numerical method of lines (MOL). The governing partial differential equations with boundary conditions were transformed into a system of ordinary differential equations (ODEs) using centered finite differences for the spatial derivatives [16]. The resulting set of ordinary

differential equations was solved in FORTRAN using the ODE solver package LSODES [17]. In the calculations the number of grid points was 81 × 81. Higher values of the internal node points did not cause any change in the results.

Results and discussion

Effect of sample composition on the reaction behaviour

The variation of the initial composition of the reactive green body, i.e. the $ZrAl_3/ZrSi_2$ mass ratio, leads to different phase compositions of the final sintered ceramic. Three starting compositions, which result in the formation of (i) Al_2O_3–ZrO_2 ceramics ($ZrAl_3/ZrSi_2$ = 100/0 mass%), (ii) Al_2O_3-mullite-ZrO_2 ceramics ($ZrAl_3/ZrSi_2$ = 80/20 mass%) and (iii) $ZrSiO_4$-based ceramics ($ZrAl_3/ZrSi_2$ = 0/100 mass%), were chosen to investigate the effects of sample composition on the reaction behaviour. The model parameters used in the calculations are summarised in Table 2. Unless otherwise stated, samples sizes of 3 mm in radius and 6 mm in height were used and the physical parameters assume the values given in Table 2. The expansion coefficient Z was estimated from porosity measurements of samples which were oxidized at different temperatures. The sintering parameters E_s and A_s were estimated from independent dilatometry measurements of pre-oxidized $ZrSi_2$ samples. The sintering parameters and the expansion coefficient were taken constant for all sample compositions to get comparable results. The effects of different sintering parameters on the reaction behaviour are studied in a following section.

Figure 2a–c show simulated TG and DTA, i.e. temperature difference curves ($\Delta T = T_{\text{average}} - T_{\text{furnace}}$), for the three initial compositions with a heating rate of 2 °C/min

Table 2 Values for model parameters used in the calculations

Quantity	Symbol	Value
Heat of reaction ($ZrAl_3$)	Q_{ZrAl3}	19.76×10^6 J/kg
Heat of reaction ($ZrSi_2$)	Q_{ZrSi2}	18.99×10^6 J/kg
Gas constant	R	8314 J/kmolK
Density $ZrAl_3$	ρ_{ZrAl3}	4120 kg/m^3
Density $ZrSi_2$	ρ_{ZrSi2}	4870 kg/m^3
Density O_2	ρ_{O2}	0.27 kg/m^3
Stefan-Boltzmann coefficient	σ	5.67×10^{-8} W (m^2 K^4)$^{-1}$
Emissivity	ε	0.99
Heat transfer coefficient	h	40 W/m^2 K
Molecular mass of O_2	M_{O2}	32 g/mol
Pore radius	r_{pore}	100×10^{-9} m
Initial porosity	ε_m	0.40
Mass transfer coefficient	k_g	0.006 m/s
Expansion coefficient	Z	1.1
Activation energy for sintering	E_s	423 kJ/mol
Pre-exponential factor for sintering	A_s	$10 \times 10^{10.26}$ s^{-1}

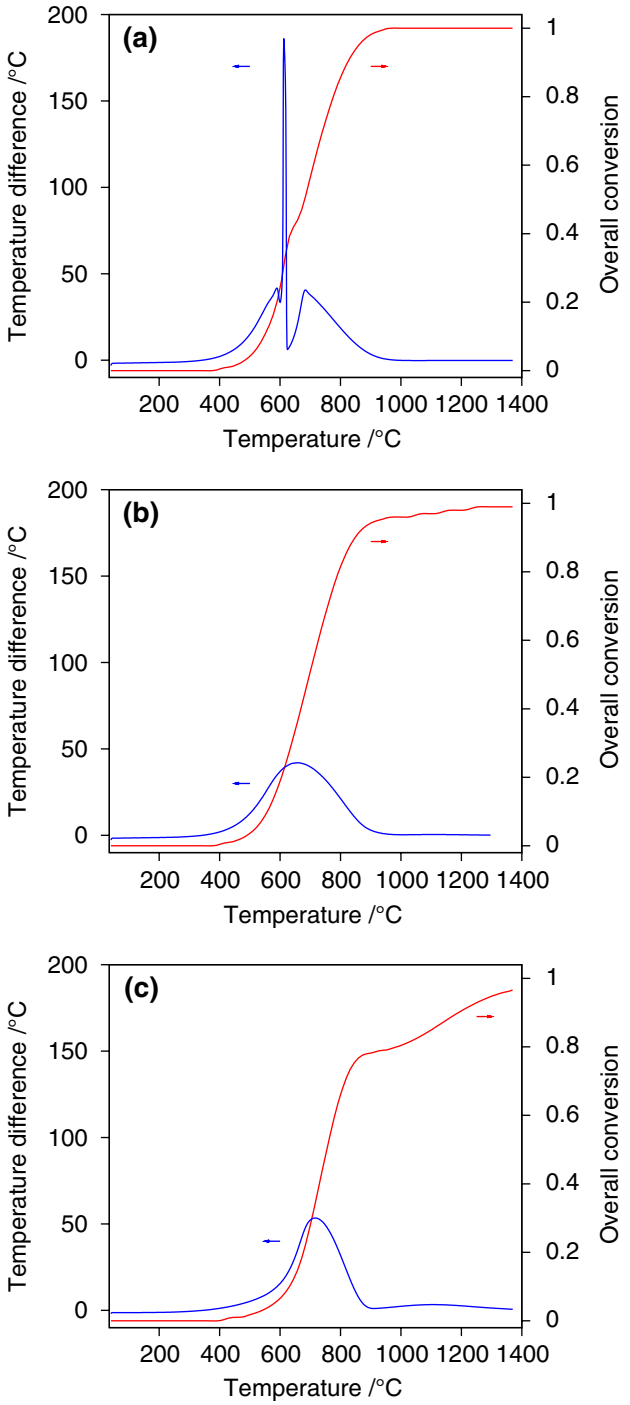

Fig. 2 Simulated TG/DTA curves for different sample compositions of $ZrAl_3/ZrSi_2$ green bodies (R = 3 mm, H = 6 mm, heating rate: 2°C/min). **a** $ZrAl_3/ZrSi_2$: 100/0 mass%, **b** $ZrAl_3/ZrSi_2$: 80/20 mass%, **c** $ZrAl_3/ZrSi_2$: 0/100 mass%

up to a temperature of 1,400 °C. The oxidation of the pure $ZrAl_3$ sample leads to a sharp exothermic peak located at approximately 620 °C. The high temperature increase of about 180 °C in the sample is caused by the chemical heat generated from the oxidation reaction which exceeds the heat losses to the surroundings and results in an increased reaction rate. Due to the depletion of oxygen in the void space the reaction slows down and the oxidation proceeds kinetically controlled up to temperatures of 1,000 °C where the reaction is finally completed. When 20 mass% $ZrSi_2$ are added to the pure $ZrAl_3$ powder, the TG and DTA curves shown in Fig. 2b are obtained. A broad ΔT peak centered at 670 °C with a maximum value of approximately 40 °C can be observed. At 1,400 °C the oxidation of the 80/20 sample is nearly completed and no excessive self-heating occurs during the course of reaction. This is due to the lower heat release because of the slower oxidation kinetics of the silicide. The simulated TG curve for the pure $ZrSi_2$ powder compact reproduces the typical multi-step oxidation behaviour of this intermetallic compound. Compared to the $ZrAl_3$ sample no thermal runaway occurs because the heat generated by the oxidation reaction can be transferred rapidly enough to the surroundings. Two ΔT peaks corresponding to the two main oxidation steps of the $ZrSi_2$ oxidation reaction at 730 and 1,030 °C can be observed in DTA curve. The second oxidation step is associated with the oxidation of the intermediate oxidation product and at 1,400 °C oxidation of the sample is not completed, which is due to the onset of sintering retarding the oxidation reaction. For complete conversion of the silicide to the corresponding oxides higher temperatures and/or isothermal hold times at elevated temperatures are necessary.

Effect of the heating rate

The effects of different linear heating rates on the predicted reaction behaviour of powder compacts with composition (i), (ii) and (iii) (see last paragraph) are shown in Fig. 3. Different heating rates ranging from 1 and 5 °C/min were used in the calculations. As can be seen from Fig. 3a–b, the oxidation behaviour of $ZrAl_3$ compacts is very sensitive to the applied heating rate. To high a heating rate causes self-accelerated oxidation behaviour with steep increases in the TG curves associated with high temperature excursions. Similar reaction behaviour can be observed for the $ZrAl_3$/$ZrSi_2$ mixture. A heating rate of 5 °C/min leads to an uncontrolled intense oxidation with steep temperature excursions. Lower heating rates show no excessive self-heating of the samples. The oxidation behaviour of the zirconium silicide powder compact is less violent compared to that of the zirconium aluminide. The silicide sample shows no self-acceleration. Only an increased sample temperature due to the heat release during the oxidation reaction can be noticed.

These results demonstrate that the heating rate has to be carefully adjusted to avoid runaway reactions and oxygen-limited reaction behaviour which lead to the formation of steep composition gradients, which in turn may result in sample cracking and bloating. Figure 4 shows a calculated TG curve for a $ZrSi_2$ sample with a modified heating schedule leading to a kinetically controlled uniform reaction of the sample with an almost constant weight gain rate and low temperature excursions. Up to a temperature of 600 °C a relatively high heating rate of 6 °C/min is used. A low heating rate of 0.9 °C/min in the temperature range where the reaction rate has its maximum, i.e. 600–800 °C, allows the reaction to proceed in a controlled manner and only slight temperature difference are predicted. Finally a high heating rate of 10 °C/min up to 1,300 °C accelerates the reaction and after the hold time of 4 h the oxidation of the sample is completed. With this modified heating cycle the reaction occurs at low temperatures and there is sufficient time for completion of the reaction prior to sintering.

Effects of sintering

The sintering behaviour of ceramics can be modified by using suitable sintering additives. With the help of these additives the required sintering temperature for full densification can be effectively lowered. This is of practical importance particularly for the fabrication of net shape reaction bonded ceramic parts as described in [4], where sintering additives such as SiO_2, Al_2O_3 and MgO are typically used in combination with reactive $ZrSi_2$ to modify the sintering behaviour of the product phase and lower the required sintering temperature. The effect of lowering the onset of sintering and therefore decreasing the temperature required for full densification can be assessed by decreasing the activation energy or increasing the pre-exponential factor for sintering. When the single change of the pre-exponential factor from $\lg(A_s/s^{-1}) = 10.23$ to $\lg(A_s/s^{-1}) = 11.0$ or $\lg(A_s/s^{-1}) = 12.0$ is introduced to the parameters in Table 2, TG curves shown in Fig. 5 are obtained. The calculations were made for $ZrSiO_4$-based ceramics (composition (iii)) because in this case higher oxidation temperatures are necessary for complete oxidation and therefore, the effect of sintering on the reaction behaviour will be more evident. The increase of the pre-exponential factor leads to a slowdown of the oxidation reaction and a decrease in the overall conversion. Incomplete oxidation of the samples is due to a decrease of the effective diffusion coefficient during the course of the reaction and finally to complete pore closure at elevated temperatures. For a value of the pre-exponential factor of $\lg(A_s/s^{-1}) = 12.0$ complete pore closure takes place at a

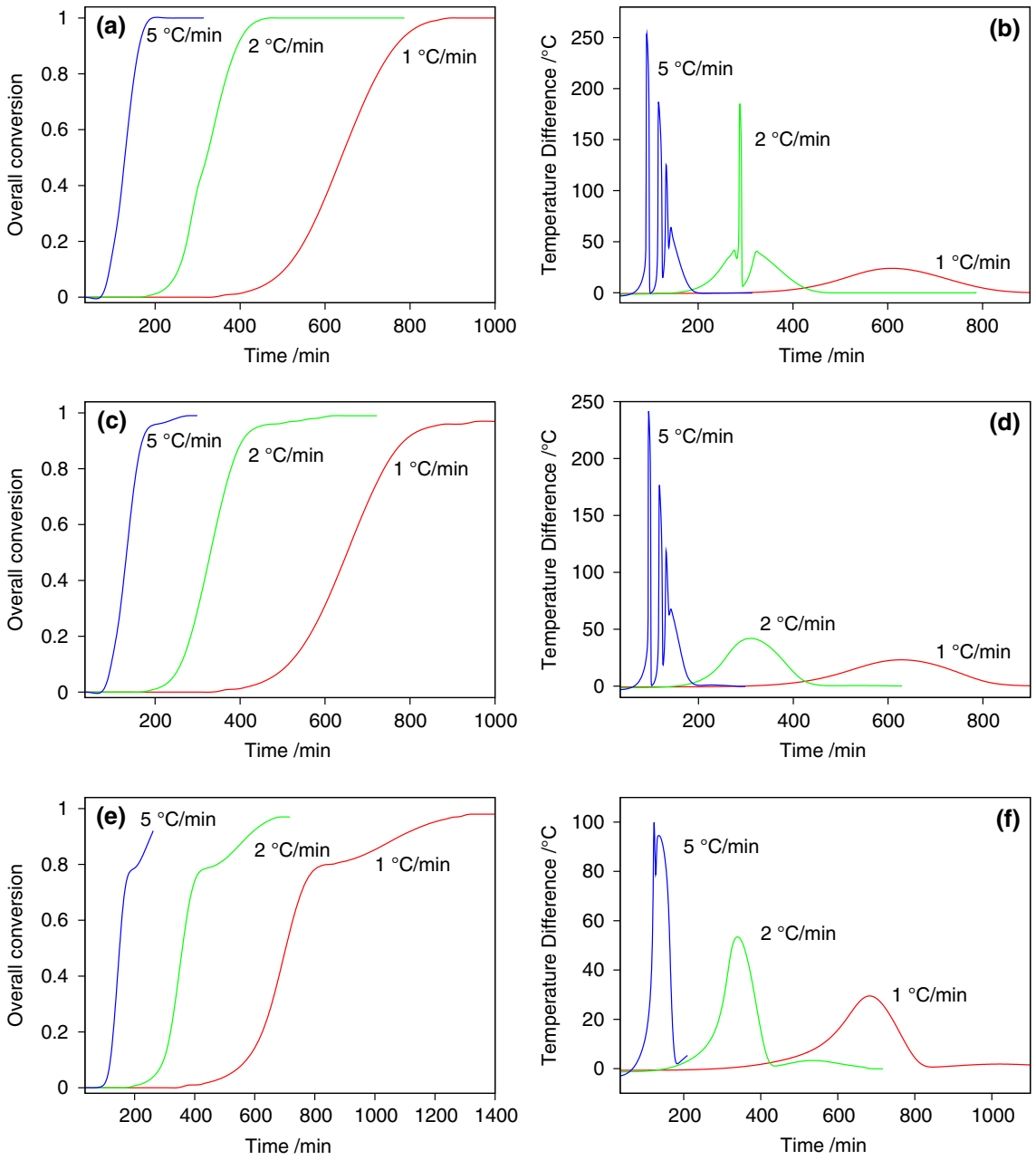

Fig. 3 Effect of different linear heating rates on the reaction behaviour of $ZrSi_2$ green bodies ($R = 3$ mm, $H = 6$ mm)

temperature of approximately 1,200 °C, which results in a plateau in the overall conversion curve at about 0.8, as can be seen in Fig. 5. This incomplete oxidation behaviour can be visualized by the evolution of the concentration profiles of the final reaction product of the $ZrSi_2$ oxidation ($ZrSi_2$-B). This is shown in Fig. 6 for a value of the pre-exponential factor $\lg(A_s/s^{-1}) = 12.0$ and a heating rate of 5 °C/min. Up to temperatures of approximately 860 °C reaction takes place throughout the sample and only slight concentration gradients can be observed. With increasing temperature oxygen is quickly consumed and locally depleted because oxygen supply is hindered by the onset of sintering. As can be seen from the contour plots in Fig. 6, steep concentration gradients are developed and finally oxidation is confined to the outer regions of the sample. At a temperature of approximately 1,200 °C all pores are removed and there is no more oxygen available in the sample for the oxidation to proceed. At the end of the heating cycle the sample consists of two distinct regions: a partially oxidized core consisting of the intermediate and final oxidation products and a fully oxidized thin outer shell.

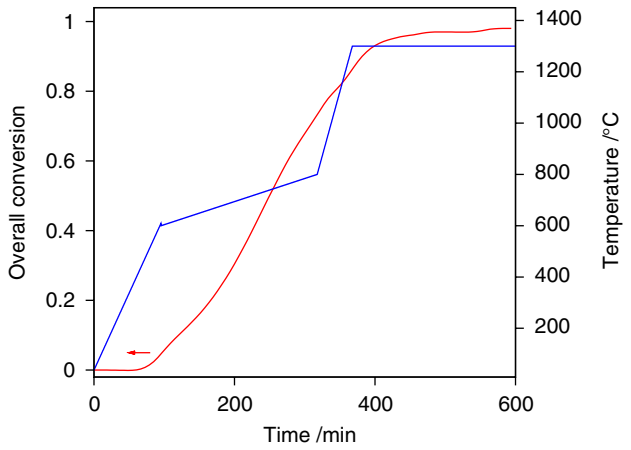

Fig. 4 Simulated TG curve (6 °C/min → 600 °C, 0.9 °C/min → 800 °C, 10 °C/min → 1,300 °C 4 h) for $ZrSi_2$ green bodies (R = 3 mm, H = 6 mm)

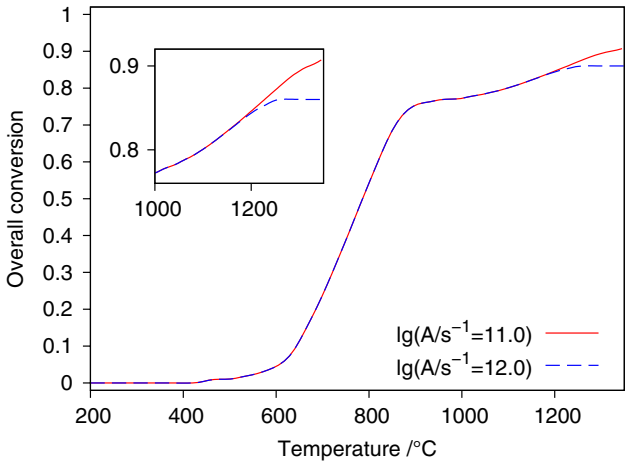

Fig. 5 Effect of the pre-exponential factor for sintering A_s on the degree of reaction. Simulated TG curves for $ZrSi_2$ green bodies (R = 3 mm, H = 6 mm) with different pre-exponential factors (heating rate: 5 °C/min)

During reaction-sintering two competing processes with different Arrhenius-type temperature dependence take place simultaneously: (a) the oxidation of the intermetallic powder particles and (b) sintering of the reacting green body. Therefore, for homogeneous and complete oxidation throughout the sample, it is necessary that the oxidation takes place at a temperature range where the sintering rate of the compact is much slower than the oxidation rate of the powder particles. Then, there is enough void space for oxygen diffusion and the diffusion through the pore structure is fast compared to the chemical oxidation reaction of the intermetallics. Thus, an oxygen-limited reaction with the formation of steep concentration gradients and typical shrinking-core reaction behaviour with possible pore closure prior to complete oxidation can be avoided.

Comparison with experiments

To compare the predictions of the 2D finite difference model with the reaction behaviour of real $ZrAl_3/ZrSi_2$ compacts, we performed thermogravimetric experiments with cylindrical samples. For the setup of the thermogravimetric experiments see [7]. Samples with about 6 mm in diameter and 8 mm height were investigated. A sample composition of $ZrAl_3/ZrSi_2$ = 80/20 mass% was chosen for validation of the model. The results of the thermogravimetric measurements together with the simulated data for heating rates of 2 and 5 °C/min are presented in Fig. 7. As can be seen, the experimental data can be reproduced very well by the 2D reaction-diffusion model. However, in the calculated temperature difference curves, which were scaled by a constant factor to match the measured DTA curves, the first sharp temperature peak is located approximately 50 °C lower than the measured DTA peak. This can be due to the simplifications of the model

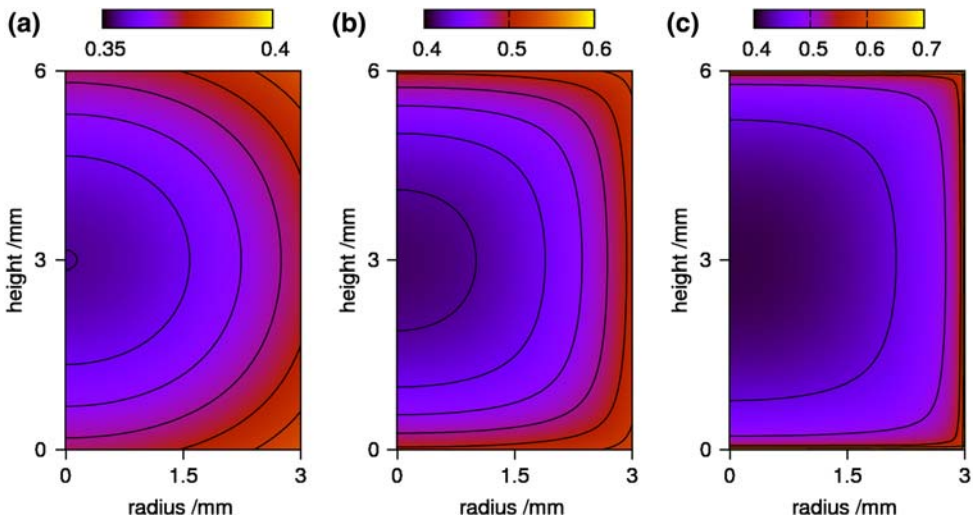

Fig. 6 Contours of the final oxidation product at different time steps corresponding to Fig. 5 (lg(A_1/s^{-1}) = 12.0). Only one half of the cylindrical sample is shown. **a** t = 227 min, T = 860 °C, **b** t = 240 min, T = 927 °C, **c** t = 253 min, T = 994 °C

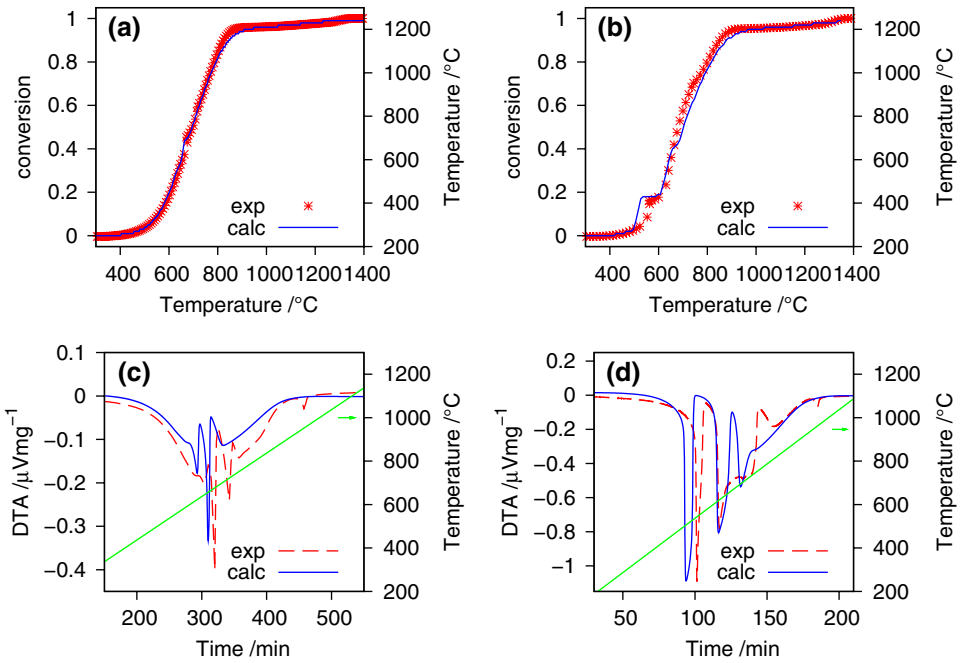

Fig. 7 Comparison of experimental and model-predicted TG/DTA curves of cylindrical green compacts with composition $ZrAl_3/ZrSi_2 = 80/20$ mass%. (**a**, **c**) Heating rate $\beta = 2$ °C/min ($\varnothing = 6$ mm, $H = 8.7$ mm) and (**b**, **d**) heating rate $\beta = 5$ °C/min ($\varnothing = 6$ mm, $H = 8.0$ mm)

und the unknown heat transfer parameters in the thermal analyzer.

Conclusions

A two-dimensional kinetic model for reaction-sintered oxide ceramics based on exothermic gas-solid reactions of the intermetallics $ZrAl_3$ and $ZrSi_2$ is developed, which enables the prediction of the progress of reaction and temperature distributions in the reactive green bodies. Complex multi-stage kinetics for the description of the oxidation reactions of the powder particles as well as a simple model for the evolution of the pore structure during the oxidation are incorporated in the model. The effects of sample composition and sintering parameters on the oxidation behaviour of the reacting green bodies are investigated. It is shown that the onset of sintering can result in shrinking-core type reaction behaviour with oxygen transport through the porous matrix as the rate determining step. This reaction behaviour is likely to result in an incomplete oxidation of the sample due to pore closure. The model is validated by comparing the simulation results with experimental thermogravimetric data of the oxidation of $ZrSi_2$ powder compacts. The model is able to predict the reaction behaviour of the reactive green bodies and can therefore be used as a tool for thermal process optimization for the fabrication of reaction-bonded oxide ceramics in the system Al_2O_3–SiO_2–ZrO_2.

References

1. Hlavacek V, Puszynski JA. Chemical engineering aspects of advanced ceramic materials. Ind Eng Chem Res. 1996;35:349–77.
2. Hennige VD, Haußelt J, Ritzhaupt-Kleissl H-J, Windmann T. Shrinkage-free $ZrSiO_4$-ceramics: characterisation and applications. J Eur Ceram Soc. 1999;19:2901–8.
3. Geßwein H, Binder JR, Ritzhaupt-Kleissl H-J, Haußelt J. Fabrication of net shape reaction bonded oxide ceramics. J Eur Ceram Soc. 2006;26:697–702.
4. Ritzhaupt-Kleissl H-J, Binder JR, Gietzelt T, Kotschenreuther J. Net shape reaction bonded ceramic micro parts by mechanical microstructuring. Adv Eng Mater. 2006;8:983–8.
5. Burnham AK, Dinh LN. A comparison of isoconversional and model-fitting approaches to kinetic parameter estimation and application predictions. J Therm Anal Calorim. 2007;89:479–90.
6. Roduit B, Folly P, Berger B, Mathieu J, Sarbach A, Anders H, et al. Evaluating SADT by advanced kinetics-based simulation approach. J Therm Anal Calorim. 2008;93:153–61.
7. Geßwein H, Binder JR, Ritzhaupt-Kleissl H-J, Haußelt J. Reaction-diffusion model for the reaction bonding of alumina-zirconia composites using the intermetallic compound $ZrAl_3$. Thermochim Acta. 2006;451:139–48.
8. Brown ME, Dollimore D, Galway AK. In: Bamford CH, Tipper CFH, editors. Comprehensive chemical kinetics, Vol. 22, Reactions in the solid state. Amsterdam: Elsevier; 1980, p. 41.
9. Geßwein H, Binder JR. Thermokinetic study of the oxidation of $ZrAl_3$ powders. Thermochim Acta. 2006;444:6–12.
10. Geßwein H, Pfrengle A, Binder JR, Haußelt J. Kinetic model of the oxidation of $ZrSi_2$ powders. J Therm Anal Calorim. 2008;91:517–23.
11. Hulbert SF. Models for solid-state reactions in powdered compacts – a review. J Br Ceram Soc. 1969;6:11–20.
12. Dandekar HW, Puszynski JA, Hlavacek V. Two-dimensional numerical study of cross-flow filtration combustion. AIChE J. 1990;36:1649–60.

13. Ku W, Gregory OJ, Jennings HM. Computer simulation of the microstructure developed in reaction-sintered silicon nitride ceramics. J Am Ceram Soc. 1990;73:286–96.
14. Ramachandran PA, Smith JM. Effect of sintering and porosity changes on rates of gas-solid reactions. Chem Eng J. 1977;14: 137–46.
15. Kim KK, Smith JM. Diffusion in nickel oxide pellets – effects of sintering and reduction. AIChE J. 1974;20:670–8.
16. Smith DD. Numerical solution of partial differential equations: finite difference methods. Oxford Applied Mathematics and Computing Science. Oxford: Clarendon Press; 1985.
17. Hindmarsh AC. ODEPACK, A systematized collection of ODE solvers. In: Stepleman RS, editor. Scientific computing, Vol. 1, IMACS transactions on scientific computation. Amsterdam: North-Holland; 1983, p. 55–64.
18. Opfermann J. Kinetic analysis using multivariate non-linear regression. J Therm Anal Calorim. 2000;60:641–58.